Research Article

Scalable Manufacturing of Bending-Induced Surface Wrinkles

Xu A. Zhang, Yijie Jiang, R. Bharath Venkatesh, Jordan R. Raney, Kathleen J. Stebe,* Shu Yang,* and Daeyeon Lee*

Cite This: *ACS Appl. Mater. Interfaces* 2020, 12, 7658−7664

Read Online

ACCESS | Metrics & More | Article Recommendations | Supporting Information

ABSTRACT: The wide range of textures that can be generated via wrinkling can imbue surfaces with functionalities useful for a variety of applications including tunable optics, stretchable electronics, and coatings with controlled wettability and adhesion. Conventional methods of wrinkle fabrication rely on batch processes in piece-by-piece fashion, not amenable for scale-up to enable commercialization of surface wrinkle-related technologies. In this work, a scalable manufacturing method for surface wrinkles is demonstrated on a cylindrical support using bending-induced strains. A bending strain is introduced to a thin layer of ultraviolet-curable poly(dimethylsiloxane) (UV-PDMS) coated on top of a soft PDMS substrate by wrapping the bilayer around a cylindrical roller. After curing the UV-PDMS and subsequently releasing the bending strain, one-dimensional or checkerboard surface wrinkles are produced. Based on experimental and computational analyses, we show that these patterns form as a result of the interplay between swelling and bending strains. The feasibility of continuous manufacturing of surface wrinkles is demonstrated by using a two-roller roll-to-roll prototype, which paves the way for scalable roll-to-roll processing. To demonstrate the utility of these textures, we show that surface wrinkles produced in this manner enhance the light harvesting and thus efficiency of a solar cell at oblique angles of illumination due to their strong light scattering properties.

KEYWORDS: surface wrinkles, scalable manufacturing, solar cells, surface instability, roll-to-roll manufacturing
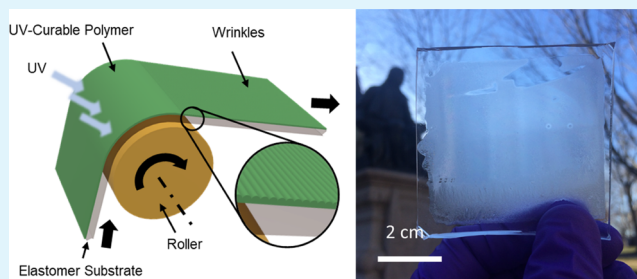
1. INTRODUCTION

Wrinkling is a ubiquitous surface phenomenon that occurs over a wide range of length scales from kilometers to nanometers. Wrinkling occurs via surface buckling when a bilayer with different mechanical properties undergoes a compressive strain. There has been a plethora of reports that describe the mechanisms, fabrication methods, and applications of buckling-induced surface wrinkles.[1−4] For real-world applications, micro/nanoscale wrinkles present a powerful platform to impart useful properties to the surface. For example, surface wrinkles can guide cell alignment and protein expression, which are important to the design and development of medical implants.[5−7] Surface wrinkles can display antibacterial and antifouling properties attributed to their complex surface topography.[8] Because wrinkles provide an extra area that can accommodate bending and stretching, wrinkled surfaces can serve as substrates for flexible electronic devices.[9−11] Surface wrinkles have been used as templates for colloidal self-assembly for applications in optical metasurfaces,[12] surface-enhanced spectroscopy,[13] and strain sensing.[14,15] Reversible wrinkle formation under cyclical stretching and release has been used to dynamically manipulate light transmission,[16] liquid wetting,[17] and surface adhesion.[18] Surface wrinkling has also been used in metrology to determine the mechanical properties of thin films.[19,20]

In general, surface wrinkles formed via buckling are produced by applying a compressive strain on a bilayer system with different mechanical properties (i.e., stiffness). One widely used technique to generate surface wrinkles is to treat a stretched poly(dimethylsiloxane) (PDMS) sheet with oxygen plasma,[4,21] which oxidizes the PDMS surface to form a hard, nanometer-thin silicate layer, creating a bilayer with a large difference in Young's modulus. Upon release of the prestrain, surface wrinkles form to accommodate the released strain energy. Other techniques follow similar mechanisms, but with different material systems and strategies to induce the compressive strain, such as thermal treatment,[22] swelling,[23,24] local laser heating,[25] and ultraviolet (UV) curing.[26] Recent research involves the use of chemical oxidation[27] and wrinkled boundaries[28] among others to control wrinkle geometry.[29] Polymers with gradient cross-linking density have also been used to form wrinkles by taking advantage of the graded mechanical properties.[24] These aforementioned fabrication techniques are well established and can be used to fabricate surface wrinkles of desired features and dimensions reprodu-
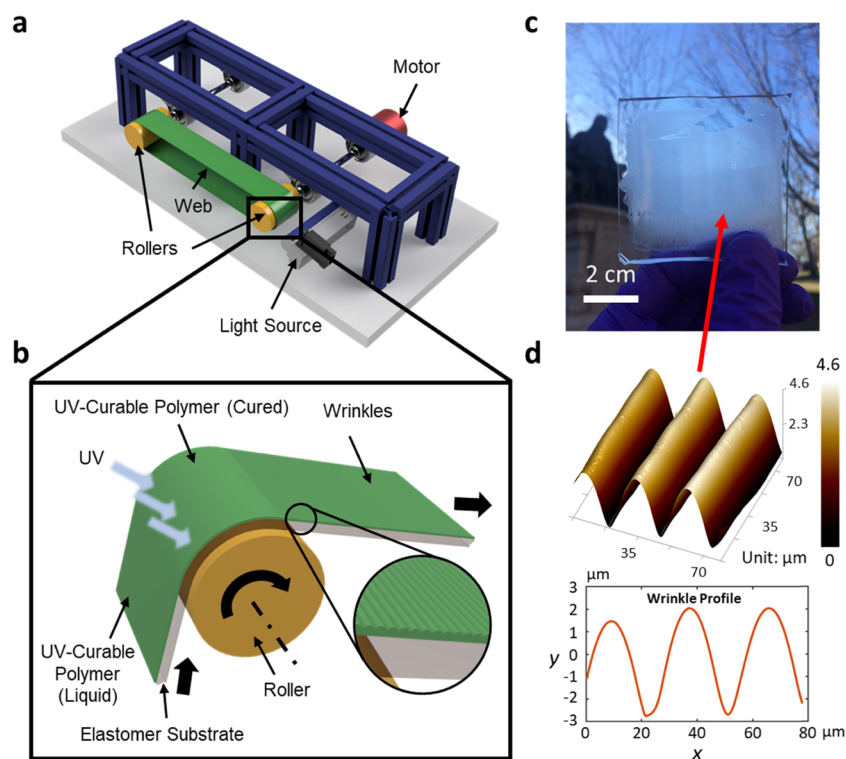
Figure 1. Bending-induced buckling concept and demonstrations. (a) Schematic illustration of the bending-induced surface wrinkle manufacturing prototype. (b) Mechanism of wrinkling. A liquid UV-curable polymer is coated on a soft elastomer sheet and is cured by UV light on the curved surface. (c) Photo of a 4×4 cm^2 surface wrinkle sample fabricated from the roll-to-roll prototype. (d) Atomic force microscope (AFM) image of the 1D sinusoidal wrinkle surface of the sample in (c). The line plot shows the cross-section of the wrinkle profile.

cibly at the nano-/micrometer scales. However, surface wrinkles are typically fabricated in a piece-by-piece manner by applying or releasing strain over the entire area of a given sample. Although suitable for small-scale proof-of-concept demonstrations, conventional methods of wrinkle formation do not easily allow for continuous fabrication of surface wrinkles, which is a major hurdle that limits the commercial applications of wrinkled surfaces.

In this work, we introduce bending-induced buckling as a scalable method of surface wrinkle formation. This technique takes advantage of the well-defined bending strain that is applied on a surface by wrapping a bilayer PDMS sample of two different stiffnesses around a cylindrical surface. Upon release of the bending strain imposed on the bilayer, wrinkles of different surface topographies are produced, including one-dimensional (1D) sinusoidal wrinkles and two-dimensional (2D) checkboard patterns. We use a combination of experimental and computational methods to understand the origin of various surface wrinkles that are formed using this method. Moreover, taking advantage of the cylindrical support that induces buckling, we develop a roll-to-roll (R2R) prototype to demonstrate the feasibility of continuous manufacturing of surface wrinkles. Although a plate-to-roll (P2R) method has been reported to form 1D wrinkles continuously,[30] our R2R method can produce wrinkles on a surface without bringing that surface in contact with another surface and can also produce both 1D and 2D surface wrinkles. The potential utility of R2R-manufactured surface wrinkles as a light scattering layer is demonstrated by substantial enhancement of light harvesting and thus the energy conversion efficiency of solar cells under oblique angles of solar illumination.

2. RESULTS AND DISCUSSION

2.1. Roll-to-Roll Manufacturing Prototype. Owing to its low cost, high speed, and versatility, R2R manufacturing is widely used in industry for large-scale production of various sheet/membrane/paper-based products. The R2R prototype based on bending-induced buckling for surface wrinkle formation is illustrated in Figure 1a (see Figure S1 for a photo of the prototype). The prototype consists of two cylindrical rollers, an elastomeric web, a cylindrical UV light source, and a driving motor. A detailed diagram of the wrinkling process is shown in Figure 1b. The elastomeric substrate made of PDMS (Sylgard 184) is first spin-coated with a thin layer of UV-curable PDMS. The bilayer sheet is wrapped onto a cylindrical roller, experiencing a bending strain. By impinging UV/Ozone (UV/O$_3$) light onto the bilayer, the wrapped portion of UV-PDMS is cured and hardened. Here, the UV/O$_3$ light is chosen because of its high-energy flux (185 and 254 nm wavelength peaks) that facilitates the rapid curing of UV-PDMS, resulting in a high degree of cross-linking. Upon the rotation of the roller, the bending strain in the substrate PDMS layer is released as the bilayer flattens, leading to the formation of surface wrinkles, which can be easily observed with the naked eye. No delamination of the bilayer is observed during processing, suggesting that the two layers have strong adhesion due to their chemical similarities. Based on this prototype, a 4 cm $\times$ 4 cm wrinkle sample is fabricated, as shown in Figure 1c (see Section 4 for more details). The wrinkled region, which covers extensive areas of the sample, appears hazy on a transparent PDMS substrate due to light scattering, which will later be used to enhance light harvesting of solar cells under oblique illumination. Figure 1d shows the atomic force microscope (AFM) image and the

cross-sectional profile of the surface wrinkles shown in Figure 1c. In this image, 1D sinusoidal surface wrinkles are apparent with the 4.6 μm height and the 28.0 μm wavelength. Examination of the entire sample area shows a roughly 7% variation in the wavelength, possibly due to the nonuniform thickness of the UV-PDMS during spin coating and gravitational flow during the R2R process.

2.2. Surface Wrinkle Library and Wrinkling Mechanism. For a given polymer thickness, the bending strain in the cured polymer should depend on the roller curvature (i.e., diameter) and the substrate thickness. To understand the effect of these two processing conditions, we prepare cylindrical rollers with diameters ranging from 8 to 30 mm using three-dimensional (3D) printing. The thickness of the PDMS substrate is varied from 1 to 4 mm. The UV-PDMS thickness is fixed at ∼10 μm. The bilayer films are then gently wrapped around a roller and fixed with an adhesive tape at both ends.

From the optical microscope images shown in Figure 2, three types of wrinkle patterns (grouped using red, green, and
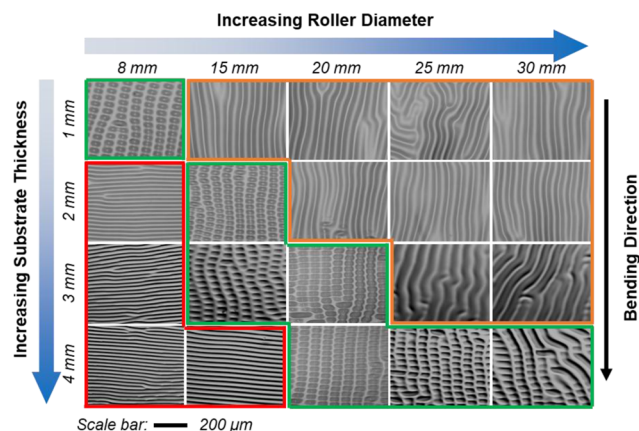
Figure 2. Wrinkle library from stationary exposure with varying cylindrical roller diameters and PDMS substrate thicknesses. The optical microscope images show three distinct types of wrinkles in red, green, and orange boxes.

orange outlines) are observed under different combinations of the substrate thickness and the roller diameter. Group red has 1D wrinkles formed perpendicular to the bending direction. Group orange also has 1D wrinkles but more or less parallel to the bending direction. These "parallel" wrinkles have larger periods than the "perpendicular" wrinkles. In the intermediate region represented in green, 2D "checkerboard" wrinkles are obtained, which can be regarded as the superposition of the parallel and perpendicular wrinkles. Since the wrinkle wavelengths in the two directions are different, the checkerboard dots appear elliptical with long axes perpendicular to the bending direction and short axes parallel to the bending direction.

Based on the buckling mechanism, the release of bending-induced strain along the bending direction in the bilayer should give rise to perpendicular wrinkles, which is indeed the case of wrinkles in the red group. However, to understand the two other types of surface wrinkles, it is necessary to investigate the wrinkling mechanism in greater detail. 2D finite element analysis (FEA) using ABAQUS is carried out to determine the bending strain field within the elastomer substrate, as shown in the left panel of Figure 3a (see details on FEA simulation in Section 4). Since the UV-PDMS coated
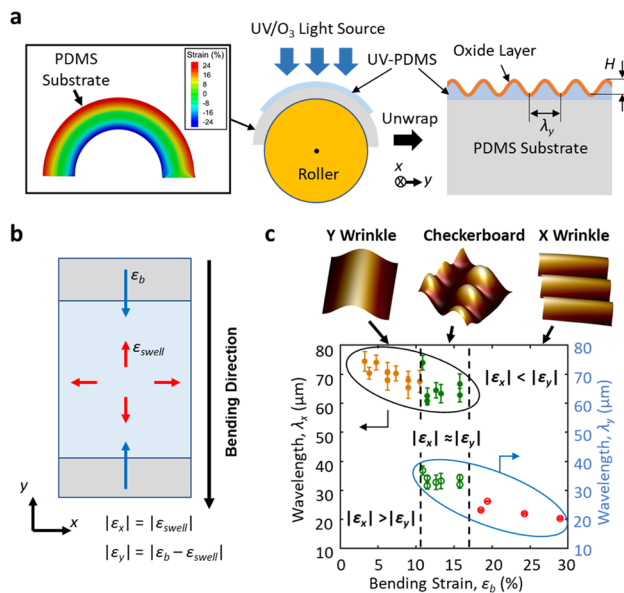
Figure 3. Wrinkling mechanism. (a) UV exposure schematic for wrinkle generation from the stationary roller. The left panel shows the bending strain distribution of the PDMS substrate using finite element analysis. Due to oxidation from the UV/O$_3$ light source, a hard oxide layer exists on the UV-PDMS layer, as shown in the right panel diagram after unwrapping. λ is the wrinkle wavelength and H is the wrinkle height. (b) Strain diagram showing bending and swelling strain states. (c) Wrinkle wavelength in x- and y-directions (λ_x and λ_y) with respect to the respective bending strains. Three distinct wrinkle types are found in three bending strain levels. The atomic force microscope (AFM) images show the typical profiles of Y wrinkles, checkerboard wrinkles, and X wrinkles.

on the PDMS substrate is liquid when the bending strain is applied, it is not explicitly included in the FEA simulation. No friction is considered in the contact area as the roller is stationary, and the film is gently laid on the roller surface without experiencing friction. FEA shows that the maximum tensile strain occurs at the top substrate surface, providing the prestrain to form surface wrinkles upon release of the bilayer from the cylindrical roller.

According to the bilayer buckling theory,[4] the wrinkle wavelength is directly related to Young's modulus ratio between the bilayer system

$$\lambda = 2\pi h \left(\frac{\overline{E}_f}{3\overline{E}_s} \right)^{1/3} \tag{1}$$

where λ is the wrinkle wavelength, h is the thickness of the top layer, $\overline{E}_f = E_f/(1 - v_f^2)$ and $\overline{E}_s = E_s/(1 - v_s^2)$, E_f and E_s are Young's moduli for the top and the substrate layers, respectively, and v_f and v_s are the Poisson's ratios for the top and the substrate layers, respectively. From the observations in Figure 2, 1D surface wrinkles with orthogonal orientations (red and orange groups) exhibit very different wavelengths and heights. Assuming a bilayer system of UV-PDMS on PDMS, a naive application of eq 1 suggests that the cured UV-PDMS film should have anisotropy in Young's moduli in orthogonal directions to explain the difference of wrinkle geometry observed in Figure 2. A prior study has shown that photopolymerization of a translating precursor layer using a cylindrical UV source can induce anisotropy in the internal structure of the cured layer.[31] However, we do not observe

anisotropy in the scanning electron microscopy (SEM) cross-sections of cured UV-PDMS. A closer examination of the wrinkling system reveals that an oxide layer exists on top of UV-PDMS, resulting from the UV ozonolysis, which is harder than the cured UV-PDMS immediately below the oxide layer (Figure S2). Similar ozonolysis on PDMS was observed in the recent work,[32] where it is used to form wrinkles with varying wavelengths. Therefore, strictly speaking, the system is composed of three layers. Since the wrinkles are only present in the UV-PDMS layer, while the PDMS substrate is flat (Figure S2b and the right panel in Figure 3a), we treat the system as a trilayer system of an oxide layer and a UV-PDMS layer atop a PDMS substrate to provide insights on the wrinkling mechanism.

The strain analysis in Figure 3b reveals two major sources of prestrain for wrinkle formation. The bending strain, due to the roller curvature, is parallel to the bending direction. Deposition and subsequent curing of UV-PDMS induce swelling of the PDMS substrate and compression of the UV-PDMS film substrate, respectively. This sequence of events, we believe, exerts an equibiaxial strain that plays an important role in the formation of the parallel and checkerboard wrinkles. The interplay between these two sources of strain determines the dominant wrinkling modes as seen in Figure 2. While PDMS has a high thermal expansion coefficient, thermal expansion as one source of prestrain is ruled out by exposing a flat sample with UV light and cooling (Figure S3a). Random wrinkles are formed without preferred orientations as shown in Figure S3b, indicating the presence of equibiaxial swelling strains rather than unidirectional thermal strains. When the bending strain is small enough to cancel the swelling strain in the y-direction, the swelling strain in the x-direction is dominant so that total strain in x, $|\varepsilon_x|$, is significantly larger than the total strain in y, $|\varepsilon_y|$. Under such conditions, Y wrinkles (parallel to the bending direction) occur, as shown in the left region of the plot in Figure 3c. As the bending strain increases to the range where $|\varepsilon_x|$ becomes comparable to $|\varepsilon_y|$, checkboard wrinkles appear, as shown in the middle region of Figure 3c. Note that checkerboard wrinkles occur only when prestrain just exceeds critical buckling strain, according to the established theory,[33] which explains the narrow window of bending strains ($\sim5\%$) that leads to the formation of checkerboard wrinkles in Figure 3c. This observation also indicates that a precise prestrain control is needed for the R2R manufacturing of checkerboard wrinkles. When bending strain further increases, the bending strain dominates so that X wrinkles (perpendicular to the bending direction) are present, as shown in the right region of Figure 3c.

As discussed above, an oxide layer forms shortly after UV/O_3 exposure, that is, the ozone oxidation occurs while the bulk of the UV-PDMS layer is not fully cured and thus remains soft. This situation leads to large Young's modulus ratio between the oxide layer and the partially cured UV-PDMS layer. From eq 1, this large Young's modulus ratio leads to a large wrinkle wavelength upon release of swelling strain. As the bottom UV-PDMS layer is further cured in the later wrinkling stages, the surface wrinkles with large wavelengths become "locked in". However, in the bending-dominant region where X wrinkles occur, the bending strain is released only after the UV-PDMS layer is fully cured, when Young's modulus difference is small, resulting in smaller wrinkle wavelengths. For the Y wrinkles, the wavelength shows no dependence on the sample width in Figure S4. However, a sample should be wide enough to allow

a few periods of wrinkles to exist. Therefore, there is a critical width (<3.0 mm) below which no wrinkles will form. The wrinkle aspect ratio (height-to-wavelength ratio) is plotted against the bending strain in Figure S5, where the higher the bending strain, the larger the aspect ratio. These results indicate that careful control over the conditions under which prestrain and curing/UV radiation are applied, wrinkle topography can be tailored over large areas.

2.3. Application of Surface Wrinkles as Optical Diffusers for Enhanced Light Harvesting. We test the utility of the large-area surface wrinkle films as optical diffusers for solar cells. With flat surfaces, reflection loss of solar light increases at oblique angles, reducing light absorption and thus conversion efficiency. One potential solution is to employ solar tracking systems so that the solar panels follow the movement of the sun to reduce reflection loss and ensure maximum solar light absorption.[34] However, this method intrinsically requires moving parts and the use of energy, which in effect increases the cost and lowers the power yield from the solar panels. One way to operate solar cells without the need for such a tracking system is to use optical diffusers. There exist many types of structured or roughened surfaces to act as optical diffusers to enhance solar cell efficiency,[35−37] and surface wrinkles can serve the same purpose with potential manufacturing scalability. Surface wrinkle films, as additional top layers between air and the solar cell, could potentially increase optical absorption by redirecting photons into oblique directions so that the resultant solar cell output could be effectively enhanced. In Figure 4a, the transmission and reflection of a
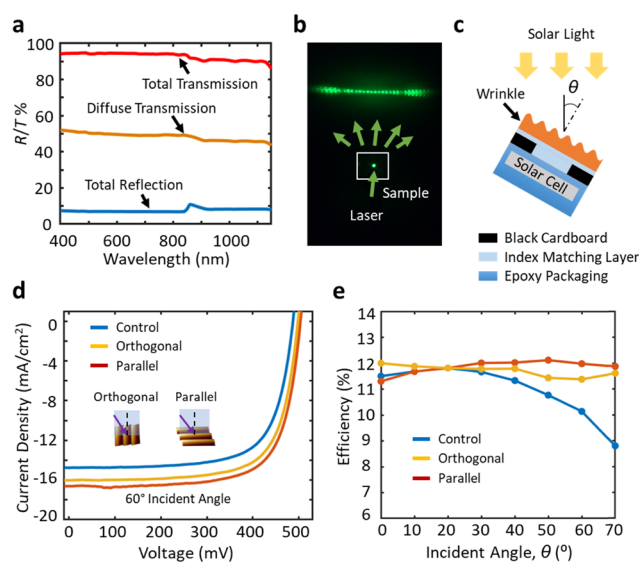
Figure 4. Optical properties of surface wrinkles and solar energy harvesting using surface wrinkles as optical diffusers. (a) Total transmission, diffuse transmission, and total reflection of the wrinkled film (the 28.0 μm wavelength and the 4.6 μm height) measured using a UV−vis−NIR spectrophotometer equipped with an integrating sphere in the normal incidence. (b) Photograph of the diffraction pattern from a 1D wrinkle film illuminated by a 532 nm laser pointer. (c) Solar cell testing setup using the solar simulator. θ is the incident angle of the solar light. (d) $I-V$ curves for the solar cell with and without the wrinkled film at 60° incident angle. "Orthogonal" and "parallel" refer to two illumination configurations for the 1D wrinkle film. (e) Solar cell efficiency at different incident angles with and without wrinkle films at orthogonal and parallel illumination configurations.

1D wrinkle film (a wavelength of 28.0 μm and a height of 4.6 μm) are shown from measurements using an integrating sphere and a UV−vis−NIR spectrophotometer with normal incidence. Diffuse transmission due to scattering accounts for roughly 50% of the transmitted light, which suggests that these surface wrinkles can indeed function as effective optical diffusers. The scattering pattern of the 1D wrinkle in Figure 4b shows that scattering light is mainly from diffraction orders.

The power conversion efficiency of the wrinkle-capped single crystalline silicon solar cell (see the setup in Figure 4c) is characterized under varying angles of solar illumination. The current−voltage (I−V) curves from the wrinkle-capped solar cell are recorded at incident angles from 0 to 70°. Comparison of I−V curves with and without the surface wrinkle diffusers at the 60° incident angle is shown in Figure 4d. The wrinkle-capped solar cell shows a higher current density than that without the wrinkles. Illumination is also performed in the orthogonal and parallel directions to wrinkle patterns, as defined in the insets of Figure 4d. The two I−V curves show small differences, possibly due to the difference in scattering patterns.

The impact of surface wrinkles on the power conversion efficiency under varying illumination angles is summarized in Figure 4e. For the solar cell with a texture-free smooth surface, the efficiency drops significantly with the increasing incident angle, due to the increased reflection loss from Fresnel reflection. With wrinkles on top of the solar cell, the transmitted light is scattered to enhance light absorption. As a result, the solar cell efficiency does not change significantly with the increasing incident angle. At the 70° incident angle, for example, the efficiency remains at ∼12% in comparison to ∼9% without the optical diffuser. In Figure S6, a simplified sun movement model relates the incident angle to time of the day. The enhancements of integrated solar efficiency for orthogonal and parallel configurations compared to bare cells are 5.6 and 7.3%, respectively. Clearly, by adding a layer of wrinkled films to solar cells as the optical diffuser, it is possible to maintain the solar cell efficiency under varying solar illumination angles, and the scalable manufacturing technology described in this work can play an important role in producing the optical diffusers that can be retrofitted onto existing solar panels.

The difference in the solar cell efficiency between parallel and orthogonal wrinkles is at most ∼1%, as shown in Figure 4e. The slight difference comes from the fact that the scattering profiles induced by parallel and orthogonal wrinkles are different. For the orthogonal configuration in Figure 4d, the angle of transmission diffractive orders increases with the incident angle of solar light. This can slightly increase the reflection loss at the solar cell surface, due to the Fresnel reflection loss. However, for the parallel configuration, the diffraction order angles remain the same as the solar incident angle increases so that the reflection loss is insensitive to the incident angle. Since the refractive index contrast between index matching oil and Si is small, the reflection loss at oblique angles is not large in general. Therefore, the solar cell efficiency difference between orthogonal and parallel is only ∼1%. While the current work focuses on the scalable manufacturing of surface wrinkles, more detailed studies about the relationships between the wrinkle morphology and the solar energy harvesting efficiency warrant future investigations.

3. CONCLUSIONS

In conclusion, a scalable manufacturing technique to fabricate surface wrinkles over a large area is demonstrated with strain engineering achieved by surface curvatures. The bending of a soft bilayer film over a cylindrical support provides the prestrain to generate surface wrinkles. UV/O_3 light is used to cure the top layer, which can be performed in ambient conditions. The interplay between bending and swelling strains can induce line and checkerboard-shaped surface wrinkles. Such a wrinkling process is demonstrated in a R2R prototype, and the utility of large-area winkles produced by this method is demonstrated by using the wrinkle as an optical diffuser to enhance light harvesting property of a solar panel under oblique solar illumination.

While this prototype provides a clear demonstration of the bending-induced buckling and its potential extension to continuous manufacturing of surface winkles, the setup can be further improved to a more sophisticated system with additional controls and functionalities. For example, tension rollers can be added to the current design for quality control. Blade coatings could be used for continuous deposition of the top layer. Also, the method can be extended to other pairs of UV-curable polymers and substrate materials. Polymer coatings with faster curing chemistry could significantly increase the production rate. With the manufacturing scalability, this technology can be potentially implemented in various applications in biomedical, electronics, and optical devices as add-on layers to enhance their performance and efficiency.

4. EXPERIMENTAL SECTION

4.1. Roll-to-Roll (R2R) Prototype. The prototype was custom-designed and assembled, as depicted in Figure S1. The prototype consists of a cylindrical UV/O_3 light source (COOSPIDER UV TUVC36), a motor (BXS230A-200S Brushless DC Motor, Oriental Motor), two rollers (MiSUMi USA), and a cooling fan (ARCTIC F8 PWM Cooling Fan). Additional parts, such as shafts, bearings, aluminum frames, a base plate, and button controllers, were purchased from multiple vendors (Amazon.com, Thorlabs, Inc., MiSUMi USA). Some fixtures of the parts and cylindrical rollers with different sizes were printed using 3D printers.

4.2. Wrinkling Experiments. PDMS (Sylgard 184, DOW Chemical Company) was mixed in a 5:1 weight ratio of the base and curing agent and cured at 60 °C for 5 h as the substrate. UV-curable PDMS (KER 4690, Shin-Etsu Chemical Co., Ltd.) was mixed in a 1:1 weight ratio of components A and B and spin-coated onto the PDMS substrate at 4000 rpm for 1 min. The coated sample was then manually laid on the curved surface of a cylindrical roller to induce prestrain. Both ends were fixed with tapes. The roller was then installed on the R2R machine with a 5 mm distance to the light source for exposures.

For the sample in Figure 1c, a large piece of the wrinkle sample was manufactured by rotating the rollers to achieve continuous exposure. After spin coating the UV-curable PDMS on the 4 cm × 4 cm PDMS substrate, the sample was installed on the two-roller machine with poly(ethylene terephthalate) (PET) sheets taped to form a closed loop around the two rollers. The exposure distance was kept at 5 mm using an 8 mm diameter roller, and the roller speed was set at 0.02 rpm for complete exposure. For samples in Figure 2, stationary exposure of 15 min was used without rotation of the roller. Surface wrinkles were characterized using an optical microscope (Carl Zeiss Microscope) and an atomic force microscope (Bruker ICON AFM) in tapping mode to determine the wavelength and the height.

4.3. Finite Element Analysis. The FEA simulations are performed using 2D plane strain models in ABAQUS (Standard 6.9). The element type of CPE8RH is used, and the PDMS is modeled as a neo-Hookean hyperelastic solid with $C_{10} = 1.1525$ MPa

and $D_1 = 7.805 \times 10^{-3}$ MPa^{-1}.[38] The initial geometries are rectangles ($w \times l$) with size determined from the thickness of PDMS, t, and roller diameters, d. The width is set as $w = t$ and changes from 1 to 4 mm, and the length is $l = \pi d/2$, with d varying from 8 to 30 mm. A symmetric boundary condition is applied at one end. At the other end, the constraint of all degree of freedom is imposed to a reference point and then a rotation of π and lateral movement of d are applied.

4.4. Optical Characterizations and Solar Cell Measurements. For optical properties, wrinkle films were characterized using a UV−vis−NIR spectrophotometer (Perkin-Elmer Lambda-750) with an integrating sphere. Solar cell I−V curves were obtained from a solar simulator (Oriel Xenon Solar Simulator, AM1.5 Global Spectra). A single-crystalline Si solar cell was used in the measurements. A thin black cardboard with the 0.5×0.5 cm^2 aperture is used to limit the illumination area on the solar cell. To prevent air bubbles between the wrinkled film and the solar cell, glycerin liquid was used as an index matching layer since it has a similar refractive index to PDMS. The whole stack was mounted on a rotational stage to change incident angles.

ASSOCIATED CONTENT

Ⓢ Supporting Information

The Supporting Information is available free of charge at https://pubs.acs.org/doi/10.1021/acsami.9b23093.

Tabletop two-roller prototype; scanning electron microscope (SEM) image; experimental setup for thermal expansion strain tests; width effect for Y wrinkle formation; surface wrinkle aspect ratio; schematic illustration of the varied incident angles (PDF)

AUTHOR INFORMATION

Corresponding Authors

Kathleen J. Stebe − *Department of Chemical and Biomolecular Engineering, University of Pennsylvania, Philadelphia, Pennsylvania 19104, United States;* ⓞ orcid.org/0000-0003-0510-0513; Email: kstebe@seas.upenn.edu

Shu Yang − *Department of Chemical and Biomolecular Engineering and Department of Materials Science and Engineering, University of Pennsylvania, Philadelphia, Pennsylvania 19104, United States;* ⓞ orcid.org/0000-0001-8834-3320; Email: shuyang@seas.upenn.edu

Daeyeon Lee − *Department of Chemical and Biomolecular Engineering, University of Pennsylvania, Philadelphia, Pennsylvania 19104, United States;* ⓞ orcid.org/0000-0001-6679-290X; Email: daeyeon@seas.upenn.edu

Authors

Xu A. Zhang − *Department of Chemical and Biomolecular Engineering, University of Pennsylvania, Philadelphia, Pennsylvania 19104, United States*

Yijie Jiang − *Department of Mechanical Engineering and Applied Mechanics, University of Pennsylvania, Philadelphia, Pennsylvania 19104, United States*

R. Bharath Venkatesh − *Department of Chemical and Biomolecular Engineering, University of Pennsylvania, Philadelphia, Pennsylvania 19104, United States*

Jordan R. Raney − *Department of Mechanical Engineering and Applied Mechanics, University of Pennsylvania, Philadelphia, Pennsylvania 19104, United States*

Complete contact information is available at:
https://pubs.acs.org/10.1021/acsami.9b23093

Author Contributions

The manuscript was written through contributions of all authors. All authors have given approval to the final version of the manuscript.

Notes

The authors declare no competing financial interest.

REFERENCES

(1) Rodríguez-Hernández, J. Wrinkled Interfaces: Taking Advantage of Surface Instabilities to Pattern Polymer Surfaces. *Prog. Polym. Sci.* **2015**, *42*, 1−41.

(2) Genzer, J.; Groenewold, J. Soft Matter with Hard Skin: From Skin Wrinkles to Templating and Material Characterization. *Soft Matter* **2006**, *2*, 310−323.

(3) Yang, S.; Khare, K.; Lin, P.-C. Harnessing Surface Wrinkle Patterns in Soft Matter. *Adv. Funct. Mater.* **2010**, *20*, 2550−2564.

(4) Chen, C.-M.; Yang, S. Wrinkling Instabilities in Polymer Films and Their Applications. *Polym. Int.* **2012**, *61*, 1041−1047.

(5) Wang, Z.; Tonderys, D.; Leggett, S. E.; Williams, E. K.; Kiani, M. T.; Steinberg, R. S.; Qiu, Y.; Wong, I. Y.; Hurt, R. H. Wrinkled, Wavelength-Tunable Graphene-Based Surface Topographies for Directing Cell Alignment and Morphology. *Carbon* **2016**, *97*, 14−24.

(6) Wang, S.; Thomas, A.; Lee, E.; Yang, S.; Cheng, X.; Liu, Y. Highly Efficient and Selective Isolation of Rare Tumor Cells Using a Microfluidic Chip with Wavy-Herringbone Micro-Patterned Surfaces. *Analyst* **2016**, *141*, 2228−2237.

(7) Zhou, Q.; Wünnemann, P.; Kühn, P. T.; de Vries, J.; Helmin, M.; Böker, A.; van Kooten, T. G.; van Rijn, P. Mechanical Properties of Aligned Nanotopologies for Directing Cellular Behavior. *Adv. Mater. Interfaces* **2016**, *3*, No. 1600275.

(8) Efimenko, K.; Finlay, J.; Callow, M. E.; Callow, J. A.; Genzer, J. Development and Testing of Hierarchically Wrinkled Coatings for Marine Antifouling. *ACS Appl. Mater. Interfaces* **2009**, *1*, 1031−1040.

(9) Wu, H.; Kustra, S.; Gates, E. M.; Bettinger, C. J. Topographic Substrates as Strain Relief Features in Stretchable Organic Thin Film Transistors. *Org. Electron.* **2013**, *14*, 1636−1642.

(10) Khang, D.-Y.; Rogers, J. A.; Lee, H. H. Mechanical Buckling: Mechanics, Metrology, and Stretchable Electronics. *Adv. Funct. Mater.* **2009**, *19*, 1526−1536.

(11) Sun, Y.; Choi, W. M.; Jiang, H.; Huang, Y. Y.; Rogers, J. A. Controlled Buckling of Semiconductor Nanoribbons for Stretchable Electronics. *Nat. Nanotechnol.* **2006**, *1*, 201−207.

(12) Mayer, M.; Tebbe, M.; Kuttner, C.; Schnepf, M. J.; König, T. A. F.; Fery, A. Template-Assisted Colloidal Self-Assembly of Macroscopic Magnetic Metasurfaces. *Faraday Discuss.* **2016**, *191*, 159−176.

(13) Pazos-Pérez, N.; Ni, W.; Schweikart, A.; Alvarez-Puebla, R. A.; Fery, A.; Liz-Marzán, L. M. Highly Uniform SERS Substrates Formed by Wrinkle-Confined Drying of Gold Colloids. *Chem. Sci.* **2010**, *1*, 174−178.

(14) Minati, L.; Chiappini, A.; Armellini, C.; Carpentiero, A.; Maniglio, D.; Vaccari, A.; Zur, L.; Lukowiak, A.; Ferrari, M.; Speranza,

G. Gold Nanoparticles 1D Array as Mechanochromic Strain Sensor. *Mater. Chem. Phys.* **2017**, *192*, 94−99.

(15) Yu, Y.; Ng, C.; König, T. A. F.; Fery, A. Tackling the Scalability Challenge in Plasmonics by Wrinkle-Assisted Colloidal Self-Assembly. *Langmuir* **2019**, *35*, 8629−8645.

(16) Lin, G.; Chandrasekaran, P.; Lv, C.; Zhang, Q.; Tang, Y.; Han, L.; Yin, J. Self-Similar Hierarchical Wrinkles as a Potential Multifunctional Smart Window with Simultaneously Tunable Transparency, Structural Color, and Droplet Transport. *ACS Appl. Mater. Interfaces* **2017**, *9*, 26510−26517.

(17) Rhee, D.; Lee, W.-K.; Odom, T. W. Crack-Free, Soft Wrinkles Enable Switchable Anisotropic Wetting. *Angew. Chem., Int. Ed.* **2017**, *56*, 6523−6527.

(18) Rahmawan, Y.; Chen, C.-M.; Yang, S. Recent Advances in Wrinkle-Based Dry Adhesion. *Soft Matter* **2014**, *10*, 5028−5039.

(19) Chung, J. Y.; Nolte, A. J.; Stafford, C. M. Surface Wrinkling: A Versatile Platform for Measuring Thin-Film Properties. *Adv. Mater.* **2011**, *23*, 349−368.

(20) Stafford, C. M.; Harrison, C.; Beers, K. L.; Karim, A.; Amis, E. J.; VanLandingham, M. R.; Kim, H.-C.; Volksen, W.; Miller, R. D.; Simonyi, E. E. A Buckling-Based Metrology for Measuring the Elastic Moduli of Polymeric Thin Films. *Nat. Mater.* **2004**, *3*, 545.

(21) Lin, P.-C.; Yang, S. Spontaneous Formation of One-Dimensional Ripples in Transit to Highly Ordered Two-Dimensional Herringbone Structures through Sequential and Unequal Biaxial Mechanical Stretching. *Appl. Phys. Lett.* **2007**, *90*, No. 241903.

(22) Bowden, N.; Brittain, S.; Evans, A. G.; Hutchinson, J. W.; Whitesides, G. M. Spontaneous Formation of Ordered Structures in Thin Films of Metals Supported on an Elastomeric Polymer. *Nature* **1998**, *393*, 146−149.

(23) Kim, H. S.; Crosby, A. J. Solvent-Responsive Surface via Wrinkling Instability. *Adv. Mater.* **2011**, *23*, 4188−4192.

(24) Guvendiren, M.; Yang, S.; Burdick, J. A. Swelling-Induced Surface Patterns in Hydrogels with Gradient Crosslinking Density. *Adv. Funct. Mater.* **2009**, *19*, 3038−3045.

(25) Qi, L.; Ruck, C.; Spychalski, G.; King, B.; Wu, B.; Zhao, Y. Writing Wrinkles on Poly(Dimethylsiloxane) (PDMS) by Surface Oxidation with a CO_2 Laser Engraver. *ACS Appl. Mater. Interfaces* **2018**, *10*, 4295−4304.

(26) Chandra, D.; Crosby, A. J. Self-Wrinkling of UV-Cured Polymer Films. *Adv. Mater.* **2011**, *23*, 3441−3445.

(27) Watanabe, M.; Mizukami, K. Well-Ordered Wrinkling Patterns on Chemically Oxidized Poly(Dimethylsiloxane) Surfaces. *Macromolecules* **2012**, *45*, 7128−7134.

(28) Ding, W.; Yang, Y.; Zhao, Y.; Jiang, S.; Cao, Y.; Lu, C. Well-Defined Orthogonal Surface Wrinkles Directed by the Wrinkled Boundary. *Soft Matter* **2013**, *9*, 3720−3726.

(29) Li, B.; Cao, Y.-P.; Feng, X.-Q.; Gao, H. Mechanics of Morphological Instabilities and Surface Wrinkling in Soft Materials: A Review. *Soft Matter* **2012**, *8*, 5728−5745.

(30) Imburgia, M. J.; Crosby, A. J. Rolling Wrinkles on Elastic Substrates. *Extreme Mech. Lett.* **2016**, *6*, 23−30.

(31) Kusama, K.; Ishinabe, T.; Katagiri, B.; Orui, T.; Shoshi, S.; Fujikake, H. Double-Layer Anisotropic Light Diffusion Films Fabricated Using a Two-Step UV Curing Technique. *Jpn. J. Appl. Phys.* **2016**, *55*, No. 042601.

(32) Li, H.; Sheng, B.; Wu, H.; Huang, Y.; Zhang, D.; Zhuang, S. Ring Wrinkle Patterns with Continuously Changing Wavelength Produced Using a Controlled-Gradient Light Field. *Materials* **2018**, *11*, No. 1571.

(33) Song, J.; Jiang, H.; Choi, W. M.; Khang, D. Y.; Huang, Y.; Rogers, J. A. An Analytical Study of Two-Dimensional Buckling of Thin Films on Compliant Substrates. *J. Appl. Phys.* **2008**, *103*, No. 014303.

(34) Lamoureux, A.; Lee, K.; Shlian, M.; Forrest, S. R.; Shtein, M. Dynamic Kirigami Structures for Integrated Solar Tracking. *Nat. Commun.* **2015**, *6*, No. 8092.

(35) Xu, Q.; Meng, L.; Wang, X. Reducing Shadowing Losses in Silicon Solar Cells Using Cellulose Nanocrystal: Polymer Hybrid Diffusers. *Appl. Opt.* **2019**, *58*, No. 2505.

(36) Hussain, S. Q.; Le, A. H. T.; Mallem, K.; Park, H.; Ju, M.; Cho, J.; Park, J.; Cho, E.; Cho, Y. H.; Kim, Y. et al. In *Advanced Light Scattering through Various Textured Glass Surface Morphologies in Thin Film Silicon Solar Cells.* IEEE 7th World Conference on Photovoltaic Energy Conversion (WCPEC) (A Joint Conference of 45th IEEE PVSC, 28th PVSEC, 34th EU PVSEC), 2018; pp 3090−3096.

(37) Tsai, M. A.; Yu, P.; Kuo, H. C. In *Potential of Thin-Film Solar Cells by Using High Haze Diffuser Superstrate.* 37th IEEE Photovoltaic Specialists Conference, 2011; pp 000683−000685.

(38) Jiang, Y.; Korpas, L. M.; Raney, J. R. Bifurcation-Based Embodied Logic and Autonomous Actuation. *Nat. Commun.* **2019**, *10*, No. 128.